Available online at www.sciencedirect.com
SCIENCE DIRECT
Catalysis Today 113 (2006) 263–269
CATALYSIS TODAY
www.elsevier.com/locate/cattod

# Understanding the atomic force microscopy image of the $V_2O_5$ and $Li_{0.03}V_2O_5$(0 0 1) surface using ab initio calculations

A.D. Sayede [a,*], C. Mathieu [b], B. Khelifa [b]

[a] LPCIA, CNRS-FRE 2485, Faculté des Sciences Jean Perrin, Rue Jean Souvraz, Université d'Artois, SP 18, 62307 Lens Cedex, France
[b] CCML, Faculté des Sciences Jean Perrin, Rue Jean Souvraz, Université d'Artois, SP 18, 62307 Lens Cedex, France

Available online 25 January 2006

**Abstract**

Single crystals of $V_2O_5$ and $Li_{0.03}V_2O_5$ were imaged in ambient conditions by atomic force microscopy (AFM). Atomic-scale resolution images are compared with total electron-density plots of the surface calculated using the ab initio HartreeFock method. The calculated oxygen charge at the $V_2O_5$(0 1 0) surface suggests an increased local reactivity of the bridging oxygens with respect to electrophilic attacks by adsorbate molecules. The intercalation of lithium has no consequence on the reactivity of the surface. This is supported by results from electrostatic potentials calculated from the cluster charge distributions.


*Keywords:* AFM; $V_2O_5$; $Li_{0.03}V_2O_5$; Electronic structure

## 1. Introduction

$V_2O_5$ is a very important material that has been extensively used as cathode material in lithium batteries and industrial catalysts [1–3]. In particular, in heterogeneous catalyst, both when used alone and when activated on a suitable oxidic support. The catalytic properties of $V_2O_5$ base catalyst depend strongly on their ability to provide oxygens reactant in oxidation of hydrocarbons. In order to understand the atomistic mechanism, it is first necessary to acquire a detailed knowledge of the real space surface structure. The scanning probe microscopy is a powerful tool for acquiring such information. In most cases, observations are interpreted by assuming that filled-state images show the more electronegative atoms, and empty-state images the more electropositive atoms. Unfortunately, this qualitative argument often leaves ambiguities regarding the composition of the termination layer and the relative positions of surface atoms. In order to limit this ambiguity, we have proposed a method to overcome these difficulties by comparing experimental scanning probe microscopy images with calculated plots of the total surface electron-density. In AFM measurements, all the electrons of the surface atoms are involved in repulsive interactions with the tip, so that the AFM image of a sample surface is described by the total electron-density plot of the surface [4,5]. Such total electron-density plots, calculated using the extended Hückel tight-binding (EHTB) electronic band-structure method [6], have been necessary to explain the observed STM and AFM images of a large number of organic conducting salts, transition-metal chalcogenides and transition-metal halides [4,5]. In ambient conditions, our previous observations of $V_2O_5$(0 0 1) single crystal surface [7,8] give result which is some different from the ideal surface as observed by Smith et al. [9]; however, it is important to notice that sample used by Smith et al. was doped with Na and it is well known that some alkali atoms remain in the first layers of the bulk [10] and so surface behaviours can be modified. Accordingly, we were interested by the investigation of the clean and lithiated $V_2O_5$(0 0 1) single crystal surface in order to examine the influence of the simplest alkali atoms (here the lithium) on the catalytic properties of the (0 0 1) plane.

## 2. The geometric structure

The crystal lattice of vanadium pentoxide, $V_2O_5$, is characterized by a layer type orthorhombic structure with layers extending parallel to the (0 0 1) net plane [11–13] and unit cell parameters defined as $a = 11.51$ Å, $b = 4.37$ Å,

* Corresponding author. Tel.: +33 321 791 771; fax: +33 321 791 717.
*E-mail address:* sayede@lens.univartois.fr (A.D. Sayede).

0920-5861/$ – see front matter © 2006 Published by Elsevier B.V.
doi:10.1016/j.cattod.2005.11.083

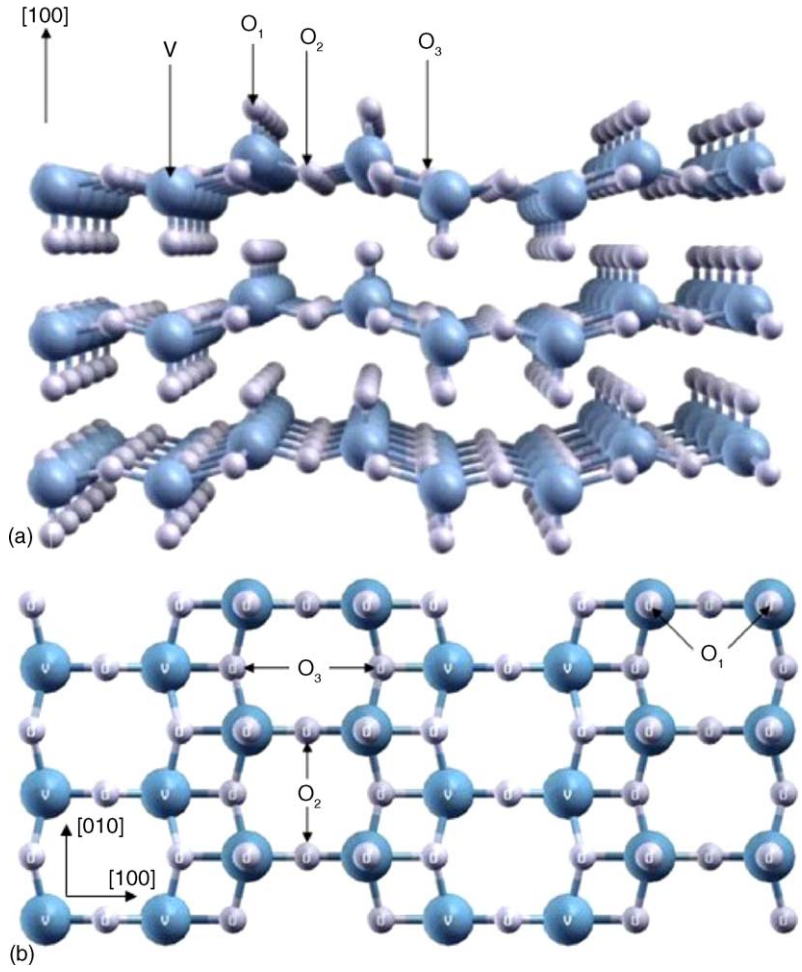


Fig. 1. (a) Perspective view of orthorhombic $V_2O_5$ crystal lattice, (b) and that projection on the (0 0 1) surface. The different types of oxygen atoms $O_1$, $O_2$ and $O_3$ are labelled.

$c = 3.56$ Å. The layers are characterized by periodic arrangements of edge and corner sharing $VO_5$ pyramids sticking out at both sides of the layer, see Fig. 1. There are three structurally different oxygen atoms, terminal (vanadyl) oxygens $O_1$ coordinated to one vanadium atom through a short bond (d(V–O) = 1.58 Å) and bridging oxygens $O_2/O_3$ coordinated to two or three vanadiums with V–O distances ranging between 1.78 and 2.02 Å. The interaction between the $V_2O_5$ layers is so small that the crystals cleave easily along the [0 0 1] direction. The $Li_xV_2O_5$ system can adopt many phases depending on temperature and lithium content $x$ [14]. The $\alpha$-$Li_xV_2O_5$ which has a low lithium content ($x < 0.1$) and the $\varepsilon$-$Li_xV_2O_5$ ($0.35 < x < 0.7$) are both stable at temperature below 400 °C. These two phases involve very little structural distortion of the bulk oxide.

## 3. Experimental procedure

### 3.1. Samples preparation

$V_2O_5$ and $Li_{0.03}V_2O_5$ single crystals have been grown by crystallization of the molten product. The powder of pure vanadium oxide was placed in a boat-shaped platinum crucible which was carried out in a quartz tube inside a furnace. A continuous purified oxygen stream was sent trough the tube. The temperature of the furnace was carried out at 50 °C/h up to a temperature higher than the melting point of the powder and kept at this temperature during 4 h to obtain a good diffusion of the different elements. In these conditions, single crystals lamella having a surface of about 20 mm × 3 mm and a thickness about 1 mm could be obtained. The faces of these obtained lamella were perfectly fat and highly reflecting. The X-ray diffraction patterns on the surface of the $V_2O_5$ single crystals show only the (0 0 1) peaks to appear indicating that these lamella are $z$-axis oriented (e.g. with the $c$-axis perpendicular to the surface).

### 3.2. AFM measurement

AFM measurements were performed in air using a Park Scientific Instruments Autoprobe CP Scanning Force Microscope that operates with an optical deflection sensor force. All imaging was performed with microfabricated $Si_3N_4$ cantilevers and microlever tips using a small repulsive force.

## 4. Method of calculation

All calculations were performed by the CRYSTAL98 code [15–17], based on ab initio Hartree-Fock methods with localized atomic-like basis functions (linear combination of atomic orbitals). The radial factors of atomic orbitals are expressed as linear combination of Gaussian-type functions of the electron–nucleus distance. We choose to use effective core pseudopotential (ECP) for the basis sets of the V and O atoms, while Li was treated at an all electron level. Hay and Wadt large core [18] and Durand and Barthelat [19] pseudopotential were employed for vanadium and oxygen, respectively. The 3d, 4sp electrons were described explicitly by 3s; 2p; 5d/3s; 2p; 3d valence basis sets for V. The Gaussian valence basis set is [Durand]-41G for oxygen, and 6-1G for Li. Numerical approximations are introduced in the evaluation of the Coulomb and exchange series for infinite systems. In the CRYSTAL code, the accuracy is controlled by a set of ''cut-off'' tolerances (see [16] for details); the values we have chosen (8, 7, 8, 8, 16) reduce the effect of numerical inaccuracies to a minimum. The contribution of electron correlation to the total energy, neglected in pure Hartree-Fock approximation, was evaluated by a *posterior* scheme based on correlation-only density-functional formulas [20]. The structure optimizations were performed by the LoptCG routine [21], which was based on numerical derivatives of the energy with respect to structural variables, and subsequent processing by conjugate gradients [22,23]. For calculations details, refer to our previous works [24,25]. The extended surface system is represented by a local cluster of finite size (cut out of the ideal solid) which is based on the assumption of dominantly local interatomic interactions at the surface. The basis of this approach is to treat surface cluster as fictitious molecule, with or without additional boundary conditions to take the effect of environmental coupling into account. Surface clusters are selected according to their sizes and detailed geometry. The main drawback of cluster model is the incorrect treatment of atoms at the cluster periphery, known as the embedding problem. To overcome this problem, the influence of the rest of the solid is reproduced by embedding this cluster in an array of model potentials. This is done by saturating the dangling bonds (peripheral oxygens) with hydrogen atoms to form OH groups, such that the bond order of each peripheral oxygen in its ideal bulk environment is obtained. In order to describe the interaction of lithium atoms with the (0 0 1) surface, clusters containing two physical layers are required as models. The following clusters are selected: $V_4O_{18}H_{24}$, $V_6O_{22}H_{18}$, $V_{12}O_{40}H_{28}$, which have to be considered electronically as a positive $V_4O_{18}H_{24}^{8+}$, $V_6O_{22}H_{18}^{4+}$, $V_{12}O_{40}H_{28}^{8+}$ ions in order to agree with the formal oxidation states of the constituent atoms, for more details see our previous works [24,25].

## 5. Results and discussion

Constant force image of the $Li_{0.03}V_2O_5$ surface is presented in Fig. 2. Assuming that the structure is bulk terminated, dimensions of the observed surface repeat unit are

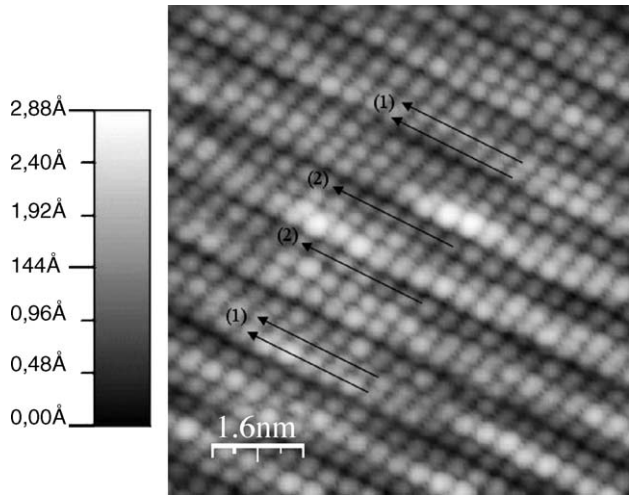


Fig. 2. AFM image of $Li_{0.03}V_2O_5$(0 0 1) surface. A 80 Å × 80 Å image. The vertical scale black to white is 2.88 Å. The arrows (1) indicate the vanadyl oxygen row and the arrows (2) indicate the presence of new rows.

11.5 Å × 3.5 Å. The lattice parameters are much closed to those of the pure $V_2O_5$. These values are analogous to data obtained by Hardy et al. [26]. In the observed AFM images, the two rows indicated by arrows (1) are considered to be rows of vanadyl oxygens. Moreover, arrows (2) indicate the presence of row between the two double rows of vanadyl oxygens. So the outermost surface is not only composed of vanadyl oxygens as in the ideal structure. These features are the same that obtained for the pure single crystals [7] (see Fig. 3). In the ideal $V_20_5$ (0 0 1) surface, the outermost surface oxygen atoms are double-bonded vanadyl ($O_1$) oxygens that reside directly on top of surface vanadium atoms, with a bond direction normal to the surface. The other surface oxygen atoms are located near the plane of the surface vanadium atoms, with their bonds almost parallel to the surface plane (see Fig. 1). The difference between the ideal structure and experimental results (with the appearance of a new row) is attributed to an adsorption

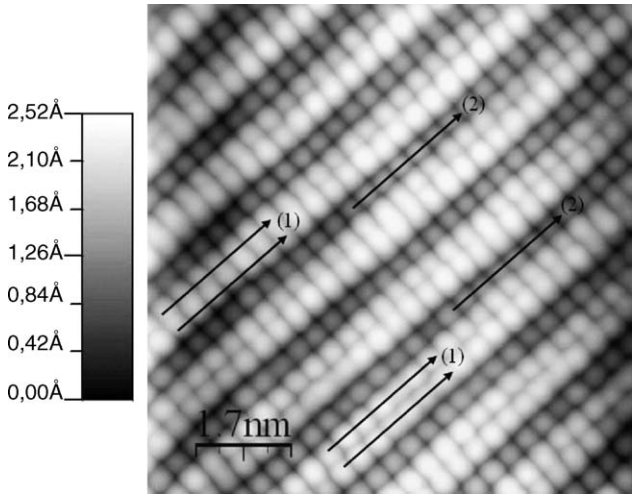


Fig. 3. AFM image of $V_2O_5$(0 0 1) surface. A 80 Å × 80 Å image. The vertical scale black to white is 2.52 Å. The arrows (1) indicate the vanadyl oxygen row and the arrows (2) indicate the presence of new rows.

Table 1
Mulliken charges and bond population for the $V_4O_{18}H_{20}$, $V_6O_{22}H_{18}$ and $V_{12}O_{40}H_{28}$ clusters

| First\|second layer atoms | $V_4O_{18}H_{20}$ | $V_6O_{22}H_{18}$ | $V_{12}O_{40}H_{28}$ |
|---|---|---|---|
| $Q(V)\|Q(V')$ | +1.868\|+1.862 | +1.848\|+1.839 | +1.841\|+1.842 |
| $Q(O_1)\|Q(O'_1)$ | −0.418\|−0.424 | −0.409\|−0.401 | −0.410\|−0.409 |
| $Q(O_2)\|Q(O'_2)$ | −1.131\|−1.129 | | −1.105\|−1.103 |
| $Q(O_3)\|Q(O'_3)$ | | −1.208\|−1.206 | −1.228\|−1.226 |
| $q_b(V–O_1)\|q_b(V–O'_1)$ | 0.376\|0.352 | 0.364\|0.361 | 0.363\|0.368 |
| $q_b(V–O_2)\|q_b(V–O'_2)$ | 2 × 0.103\|2 × 0.118 | | 2 × 0.119\|2 × 0.121 |
| $q_b(V–O_3)\|q_b(V–O'_3)$ | | 0.033\|0.031, 2 × 0.042\|2 × 0.038 | 0.043\|0.049, 2 × 0.058\|2 × 0.051 |

The atom charges $Q$ refer to vanadiums and oxygens closest to the cluster centers. For each kind of oxygen (singly coordinated $O_1$, doubly coordinated $O_2$, triply coordinated $O_3$) $q_b$(V–O) denotes the bond population with its nearest vanadium neighbours. V′ and O′ atoms belong to the bottom layer.

phenomena and not surface reconstruction. Indeed, in air, under atmospheric pressure, at room temperature, the most readily adsorbed molecule is water [8,27]. In our previous work [7], we have proposed an adsorption model which assumed that a water molecule bridges two neighbouring $O_2$ sites by means of its hydrogen atoms. Thus, the oxygen atom of the water molecule is observed between the double rows of vanadyl oxygen and so the outermost surface is not only composed of vanadyl oxygens as in the ideal structure. In this model, the oxygen site bridging two vanadium atoms seems to play an important role as active site for molecular water adsorption. Moreover, it is important to notice that lithium intercalation does not modify this behaviour.

In order to validate this experimental fact, the $V_2O_5$(0 0 1) surface and the influence of alkali atoms on this surface have been described by ab initio cluster calculations. Table 1 summarizes the results of Mulliken populations and bond populations analysis obtained for $V_4O_{18}H_{24}$, $V_6O_{22}H_{18}$ and $V_{12}O_{40}H_{28}$ clusters modelling the $V_2O_5$(0 0 1) surface. An inspection of the atomic charges in these clusters shows that the vanadium centers are always positive (+1.839$e$ to +1.868$e$) whereas all oxygens are negative as expected from basic chemical intuition. Bridging oxygen atoms are more negative (−1.103$e$ to −1.131$e$ for $O_2$ and −1.206$e$ to −1.228$e$ for $O_3$) than the terminal oxygen atom (−0.401$e$ to −0.424$e$). This indicates that the strongest ionic contribution to the V–O bonds is from vanadium atoms and bridging oxygens which agrees well with the previous published results [24,25,28–33]. The covalent character of V–O bonds is reflected by the bond populations analysis, the short V–$O_1$ bond ($q_b$ = 0.352$e$–0.376$e$) exhibits very high bond population than the V–$O_2$ and V–$O_3$ bonds. The increased charge at the bridging oxygen sites induces an increased local reactivity with respect to nucleophilic attacks which is important from a catalytic point of view. Fig. 4 displays the total valence density map in $V_4O_{18}H_{24}$ (Fig. 4a) and $V_6O_{22}H_{18}$ (Fig. 4b) clusters, for planar section parallel to the $V_2O_5$(0 0 1) surface, which confirms the mixing ionic (covalent) character of the material. For example, one can clearly see the ionic character of the V=O bond (manifested by the charge flow from the metal to vanadyl oxygen) and the covalent bond (reflected by the electron charge accumulation between these two centers). The bond between vanadium and both types of bridging oxygen is less covalent (smaller accumulation of the charge between the V and bridging oxygen centers than between V and vanadyl oxygen) but more ionic (more pronounced charge accumulation on bridging oxygen on bridging oxygens than on vanadyl ones). In order to reproduce the local lithium environment, the previous clusters ($V_4O_{18}H_{24}$ and $V_6O_{22}H_{18}$) have been chosen. One

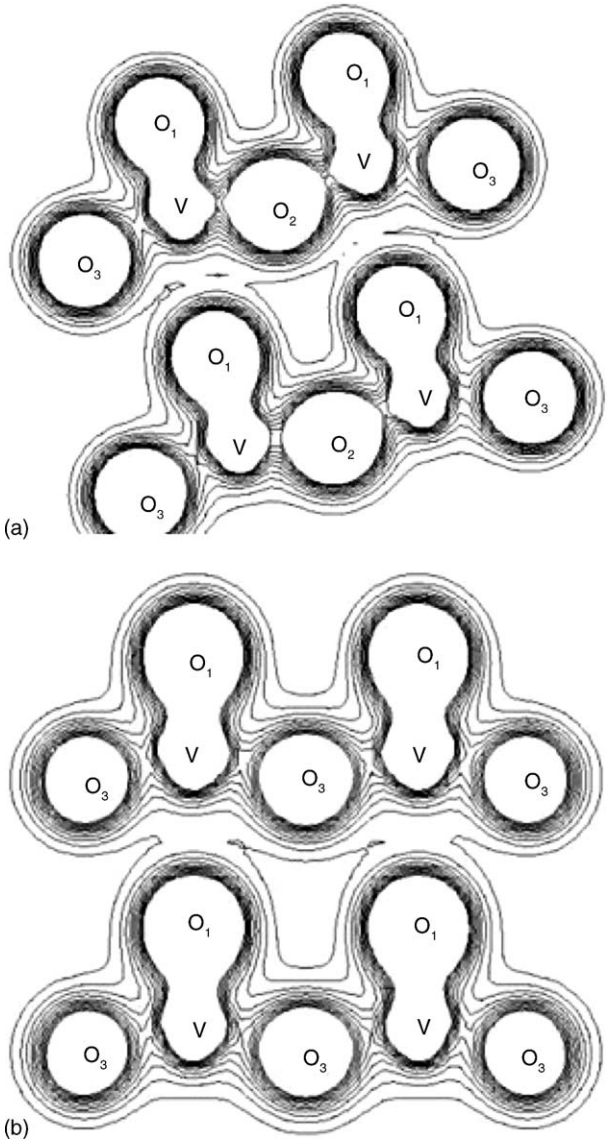


Fig. 4. Contour plots of the total charge density for the (a) $V_4O_{18}H_{24}$ cluster and (b) $V_6O_{22}H_{18}$ cluster. The contours are shown for a planar section perpendicular to the $V_2O_5$(0 0 1) surface, and refer to increments of 0.005 a.u.

Table 2
Mulliken charges and bond population for the $LiV_4O_{18}H_{20}$ and $LiV_6O_{22}H_{18}$ clusters

| First\|second layer atoms | $LiV_4O_{18}H_{20}$ | $LiV_6O_{22}H_{18}$ |
|---|---|---|
| $Q$(V)\|$Q$(V′) | +1.769\|+1.860 | Outer: +1.842\|+1.832, inner: +1.680\|+1.808 |
| $Q(O_1)\|Q(O'_1)$ | −0.429\|−0.436 | Outer: −0.410\|−0.398, inner: −0.464\|−0.429 |
| $Q(O_2)\|Q(O'_2)$ | −1.481\|−1.136 | – |
| $Q(O_3)\|Q(O'_3)$ | – | −1.694\|−1.207 |
| $Q$(Li) | +0.618 | +0.954 |
| $q_b(VO_1)\|q_b(V'O'_1)$ | 0.261\|0.323 | Outer: 0.360\|0.359, inner: 0.197\|0.283 |
| $q_b(VO_2)\|q_b(V'O'_2)$ | 2 × 0.062\|2 × 0.113 | – |
| $q_b(VO_3)\|q_b(V'O'_3)$ | – | 0.027\|0.029, 2 × 0.019\|2 × 0.035 |

The atom charges $Q$ refer to vanadiums and oxygens closest to the cluster centers. For each kind of oxygen (singly coordinated $O_1$, doubly coordinated $O_2$, triply coordinated $O_3$) $q_b$(V–O) denotes the bond population with its nearest vanadium neighbours. V′ and O′ atoms belong to the bottom layer.

lithium have been introduced between the two layers where $LiV_4O_{18}H_{24}$ and $LiV_6O_{22}H_{18}$ clusters reproduce the channel along the *a* and the *b* direction, respectively. The coordinates of the lithium atoms have been varied to check that the global minimum has been found. The starting Li coordinates are the trigonal prism between the $O_2$ or $O_3$ atoms of two successive layers, as proposed by Galy [14] following RMN measurement. $Li_xV_2O_5$ system can adopt many phases depending on temperature and lithium concentration, $x$. Our present lithiated cluster models have a low lithium content ($x \leq 0.1$), hence it is represented α-$Li_xV_2O_5$ phase, which involves very little structural distortion of the oxide, allowing us to relax just the Li coordinates. We can notice that the intercalation of lithium produces two inequivalent sets of atoms in our cluster: the inner atoms (which are in direct interaction with Li) and the outer atoms. The conventional chemistry picture is to assume that lithium is ionized to $Li^+$ with the intercalating electron reducing the metal centers from +5 to +4 states. In this work (Table 2), lithium donates 0.618 (to 0.954) *e* to the (0 0 1) surface atoms. The introduction of lithium modifies the charge of the atoms surrounding the lithium (the inner atoms). So, the charge is mainly localized on the nearest neighbours. Small reduction of the vanadium centers is observed with a maximum of 0.228*e* in the $V_6O_{22}H_{18}$ cluster (for the inner V atom of the first layer), while the amounts of additional charge on the bridging oxygen are appreciable for both doubly and triply coordinated oxygen atoms (0.350*e* for $O_2$ and 0.466*e* for $O_3$). The amount of transferred charge to the $O_1$ is very small and limited to the inner atom (0.054*e*). So, the charge transfer at the vanadia surface occurs mainly to the bridging oxygens $O_2$ and $O_3$ than the vanadyl oxygens $O_1$. With $V_2O_5$, the modification of the effective charge on the vanadium site seems to be more important for the inner atoms but for the outer atoms, the charge transfer can be neglected. As listed in Table 2, the V–$O_1$ bond order near the lithium atoms decreases from 0.364*e* to 0.197*e* with the lithium occupancy for the $V_6O_{22}H_{18}$ cluster. The same phenomena is observed with the reduction of $q_b$(V–$O_1$) from 0.376*e* to 0.261*e* in the $V_4O_{18}H_{24}$ cluster. Thus, the covalent interaction between V and $O_1$ is weakened by the lithium insertion. For the bridging oxygen $O_2$ and $O_3$ linked to the vanadium atoms near the lithium, the bond order decreases and a weakening of this bonding is observed. Fig. 5 shows the contour plot of the total charge density of the lithiated $V_2O_5$(0 0 1) surface. There is no charge accumulation between the lithium and its neighbours which seems to induce that the lithium atom is ionized. Nevertheless, the negative charging of the bridging oxygens still more pronounced than that of the terminal oxygens. This makes bridging oxygen sites more nucleophilic than vanadyl sites as on the nonlithiated

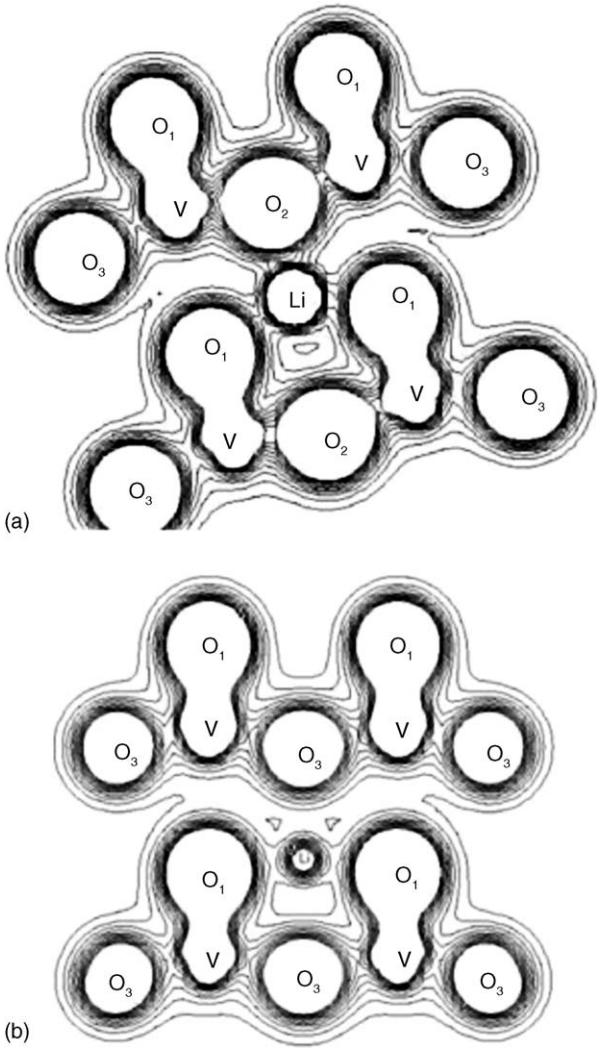


Fig. 5. Contour plots of the total charge density for the (a) $LiV_4O_{18}H_{24}$ cluster (b) $LiV_6O_{22}H_{18}$ cluster. The contours are shown for a planar section perpendicular to the $LiV_2O_5$(0 0 1) surface, and refer to increments of 0.005 a.u.

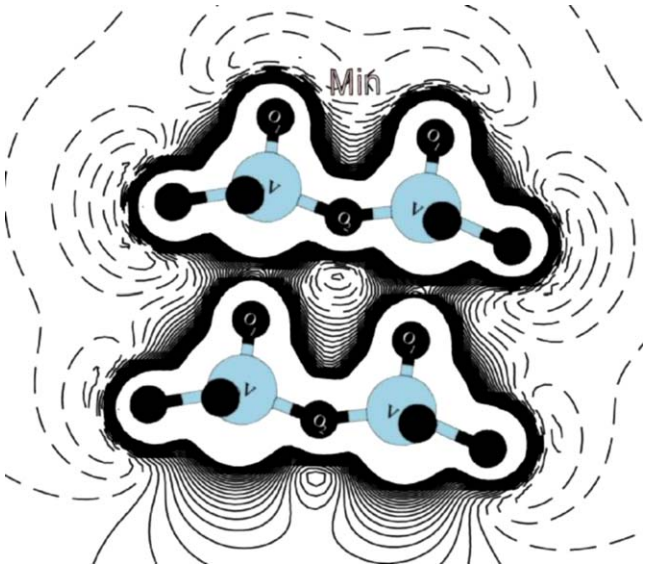


Fig. 6. Contour plots of the electrostatic potential about the $V_2O_5$(0 0 1) surface for a $V_4O_{18}H_{24}$ cluster. The contours are shown for a planar section perpendicular to the $V_2O_5$(0 0 1) surface. The contour values refer to increments of 0.01 a.u. with positive (negative) values given by solid (long dashed) lines.

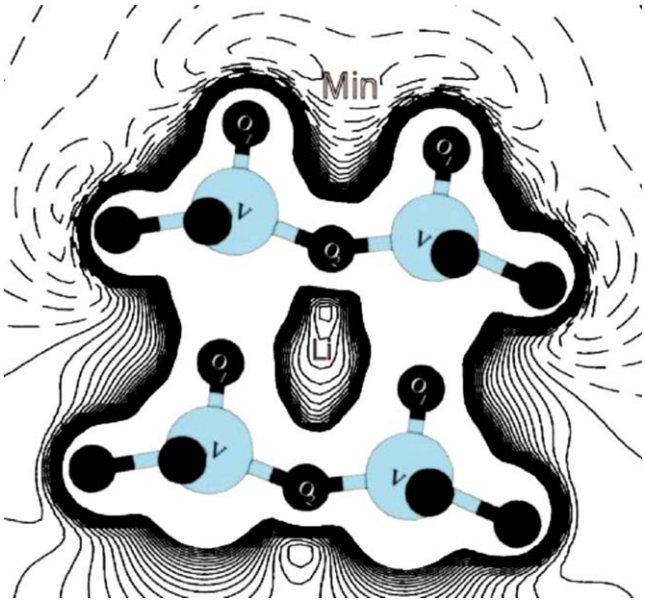


Fig. 7. Contour plots of the electrostatic potential about the $LiV_2O_5$(0 0 1) surface for a $LiV_4O_{18}H_{24}$ cluster. The contours are shown for a planar section perpendicular to the (0 0 1) $V_2O_5$ surface. The contour values refer to increments of 0.01 a.u. with positive (negative) values given by solid (long dashed) lines.

$V_2O_5$(0 1 0) surface. Electrostatic potentials computed from the cluster charge distributions can give additional informations about local charging and binding at the surface. These potentials quantify the electronic and nuclear electrostatic interaction of the clusters with an external point charge. They can be used to characterize clusters regions where adsorbates can stabilize due to electrostatic interactions.

For example, electrophilic adsorbates will be attracted to regions of negative potential while nucleophilic species stabilize near regions of positive potential. In our previous work [24] we have shown that the bridging oxygen $O_2$ plays the role of reactive site on the (0 0 1) surface. Thereby, we decide to focus our comparison between the $O_2$ centers on the lithiated and nonlithiated surfaces. Figs. 6 and 7, show the electrostatic potential contour maps computed from the cluster (nonlithiated and lithiated) charge distribution for a planar sections perpendicular to the $V_2O_5$(0 0 1) surface. These figures show that the electrostatic potential of the selected cluster yields always a sizable negative value near the oxygen sites for distances above the surface that correspond to typical molecular binding where the reaction take place. In contrast, regions close to vanadium centers result in positive potential values. In addition the plots reveal negative minima of the potential above all types of oxygens. However, the minima above the doubly coordinate oxygen $O_2$ are deeper and more pronounced. This suggests that electrophilic adparticles, like $H^+$, resulting from surface reactions, will be attracted preferentially at these sites and may form local surface bonds, which are easy to remove as suggested above by the bond analysis (Tables 1 and 2). This finding explain the resemblance between the AFM images (Figs. 2 and 3) of the clean and lithiated $V_2O_5$(0 0 1) surface, where the water molecules are attracted preferentially on the doubly bridging oxygen sites which give birth of new row of oxygen atoms (as indicated on Figs. 2 and 3). This allows us to deduce that lithium insertion does not modify the reactivity of the $V_2O_5$(0 0 1) surface.

## 6. Conclusions

By comparing experimental observations to the calculated total electron-density plots, we conclude that the $V_2O_5$(0 0 1) and $LiV_2O_5$(0 0 1) surface are not terminated only by vanadyl O atoms. Apparition of a new row of oxygen atoms is attributed to an adsorption phenomenon. Mulliken populations and bond populations analysis of the nonlithiated and lithiated surface indicate that the intercalation of lithium has no consequence on the surface reactivity. Moreover, electrostatic potentials maps computed from the cluster (nonlithiated and lithiated) charge distribution indicates that the bridging oxygen $O_2$ still play the role of the most active on the (0 0 1) surface. This suggests that electrophilic adparticles, like $H^+$, resulting from surface reactions, will be attracted preferentially at these sites and may form local surface bonds.

## References

[1] B. Grzybowska-Swierkosz, Appl. Catal. A 157 (1997) 263.
[2] H. Bosch, F. Janssen, Catal. Today 2 (1988) 369.
[3] M.S. Whittingham, J. Electrochem. Soc. Electrochem. Sci. Technol. 123 (1976) 315.
[4] S.N. Magonov, M.H. Whangbo, Adv. Mater. 6 (1994) 335.
[5] S.N. Magonov, M.H. Whangbo, Surface Analysis with STM and AFM, VCH, Weinheim, 1996.
[6] M.H. Whangbo, R. Hoffmann, J. Am. Chem. Soc. 100 (1978) 6093.
[7] A. Da Costa, C. Mathieu, Y. Barbaux, H. Poelman, G. DalmaiVennik, L. Firmens, Surf. Sci. 370 (1997) 339.

[8] C. Mathieu, S. Péralta, A. Da Costa, Y. Barbaux, Surf. Sci. 395 (1998) L201.
[9] R.L. Smith, G.S. Rohrer, K.S. Lee, D.K. Seo, M.H. Whangbo, Surf. Sci. 367 (1996) 87.
[10] J.Ph. Nogier, M. Delamar, Catal. Today 20 (1994) 109.
[11] H.G. Bachman, F.R. Ahmed, W.H. Barnes, Z. Kristallogr, Kristallgeom. Kristallphys. Kristallchem. 115 (1981) 110.
[12] H. Hanke, R. Bunert, H.G. Jetschewitz, Z. Anorg. Allg. Chem. 109 (1975) 414.
[13] L. Kihlborg, Ark. Kem. 21 (1963) 357.
[14] J. Galy, J. Solid State Chem. 100 (1992) 229.
[15] R. Dovesi, V.R. Saunders, C. Roetti, M. Causa, N.M. Harrison, R. Orlando, C.M. ZicovichWilson, CRYSTAL98 Users Manual, University of Torino, Torino, 1999.
[16] C. Pisani, R. Dovesi, C. Roetti, HartreeFock Abinitio Treatment of Crystalline Systems, Lecture Notes in Chemistry, vol. 48, Springer, Heidelberg, 1988.
[17] R. Dovesi, R. Orlando, C. Roetti, C. Pisani, V.R. Saunders, Phys. Stat. Sol. (b) 217 (2000) 63.
[18] P.J. Hay, W.R. Wadt, J. Chem. Phys. 82 (1985) 270.
[19] P. Durand, J. Barthelat, Theor. Chim. Acta 38 (1975) 283.
[20] J.P. Perdew, Y. Wang, Phys. Rev. B 45 (1992) 13244.
[21] C.M. ZicovichWilson, INSTITUTO DE TECNOLOGIA QUIMICA U.P.V.C.S.I.C., Valencia, Spain. http://www.chimifm.unito.it/teorica/crystal/LoptCG.html
[22] P.G. Mezey, Potential Energy Hypersurfaces, Elsevier, New York, 1987.
[23] W.H. Press, B.P. Flannery, S.A. Teukolsky, W.T. Vetterling, Numerical Recipes, University Press, New York, 1989.
[24] A.D. Sayede, C. Mathieu, B. Khelifa, H. Aourag, Mater. Chem. Phys. 81 (2003) 183.
[25] A.D. Sayede, B. Khelifa, M. Pernisek, C. Mathieu, H. Aourag, Solid State Ionics 166 (2004) 175.
[26] A. Hardy, J. Galy, A. Casalot, M. Pouchart, Bull Soc. Chim. Fr. 4 (1965) 1056.
[27] G. Busca, G. Ramis, V. Lorenzolli, J. Mol. Catal. 50 (1989) 231.
[28] M. Witko, K. Hermann, J. Mol. Catal. 81 (1993) 279.
[29] J. Haber, R. Tokarz, M. Witko, in: V.C. Corberan (Ed.), Stud. Surf. Sci. Catal. 82 (1994) 94.
[30] K. Hermann, A. Michalak, M. Witko, Catal. Today 32 (1996) 321.
[31] A. Michalak, M. Witko, K. Hermann, Surf. Sci. 375 (1997) 385.
[32] M. Witko, R. Tokarz, K. Hermann, Pol. J. Chem. 72 (1998) 1565.
[33] M. Witko, K. Hermannb, R. Tokarz, Catal. Today 50 (1999) 553.